RSC Advances

ROYAL SOCIETY OF CHEMISTRY

www.rsc.org/advances

A self assembled superparamagnetic nanocomposite labelled cells for noninvasive controlled targeted delivery and therapy

Ansar Ereath Beeran,[a,c] Francis Boniface Fernandez,[b,c] Annie John,[b,c] Harikrishna Varma PR[a,c*]

[a] Bioceramics Laboratory, [b]Transmission Electron Microscopy Laboratory

[c] Sree Chitra Tirunal Institute for Medical Sciences and Technology, Thiruvananthapuram-695 019, Kerala, India.

* Author for Correspondence: e-mail: varma@sctimst.ac.in

Abstract

Efficient delivery of cells to targeted sites at optimal concentration within rational limits of damage to normal tissue is a major challenge for cell delivery. With the help of magnetic nanoparticles binding to the surface of cells, it is possible to manipulate and control cell mobility using an external magnetic field. Here we demonstrate physical entrapment of magnetic nanocomposites onto cell surfaces and its manipulation by external magnetic field. Uniformly embedded nano iron oxide particles in a hydroxyapatite crystallite (HAIO) were synthesized via co-precipitation method. Physiochemical and biological evaluation of the above nano composite system showed that the HAIO containing fifty weight percentage iron oxide (HAIO50) possess excellent magnetic property and good cytocompatibility. Prussian blue staining and flow cytometric evaluation of cell – material interaction indicated uniform uptake and a dose dependent interaction. HAIO50 is found as a novel matrix for effective and cytocompatible avenue for cell separation evidenced via coulter analysis as well as fluorescent imaging of live cells. Post magnetic separation analysis of cell viability via

confocal laser scanning microscopy (CLSM) showed normal structure & proliferation of separated cells. HAIO50 may be used as an efficient matrix for magnetic non invasive manipulation and for further cell delivery applications.

1. Introduction

Superparamagnetic iron oxide nanoparticles (SPION), due to their superior inherent magnetic property, have been recognized as a potential candidate for several biomedical applications such as separation of biomolecular components[1,2] MRI contrast agents[3], hyperthermia[4] and controlled drug delivery.[5,6] Literature testifies that magnetite and maghemite are the preferred phases of SPION that are more effectively explored for such diverse biological applications.[7,8] Magnetic nanoparticle based cell therapy is one of promising area where cells are effectively labelled, separated and concentrated from a biological suspension containing multiple components and delivered to the specific site with the aid of external magnetic field.[9]

Cell therapy provides more promising solution for several disease and injuries compared to most of the conventional medicines and therapies particularly because cells can perform better physiologic as well as metabolic duties than any of the mechanical devices, recombination proteins or chemical compounds.[8,10] However, systemic administration of bare cell possesses lot of hurdles, causing significant difficulties for effective retention of the therapeutic cells at the target site. In order to achieve greater efficiency and optimum performance higher cell dose, or higher engraftment of cells is inevitable.[8,11] Nevertheless, higher cell dose induce larger systemic circulation, which in turn highlights the safety concern. Since the fundamental requirement associated with the success of cell therapy being the ability of cells to migrate and engraft,[12,13] the inability to achieve desired level of cell homing and engraftment becomes a basic challenge for cell-based therapy.

The cells tagged with SPION can migrate easily and enhance accumulation by magnetic actuation.[14] Recent literature puts forth several interesting research attempts on magnetic nanoparticle conjugated stem cell delivery towards tissue repair as well as hyperthermia applications.[15,16,17] K. Andreas *et al.,* reported the citrate modified SPION labelled stem cell delivery and its MRI trafficking.[18] Also Kyrtatos *et al.,* accounted that ferridex labelled endothelial progenitor cells efficiently targeted the arterial injury with the help of external magnetic field.[19] Basically, labelling techniques utilizes either of the two approaches (a) immobilizing magnetic nanoparticles to the cell surface[20] or (b) internalization of biofunctional magnetic nanoparticles, for example *via* endocytosis.[21] In a receptor mediated endocytosis, more particles may chance to accumulate inside the cells and chance to cell stress.[22] Therefore, surface charge enhanced nanoparticle cell labelling may be considered as a suitable option.

The satisfactory pre-requirements for magnetic nanoparticles to be used for such applications are as follows; should be stable enough to remain its physical integrity, retain its chemical stability, and sustain in the suspension state. More significantly, it should not induce any unfavoured reaction in the biological milieu; nevertheless, it should facilitate faster and efficient binding to the required biomolecular component. In addition, feasibility of large scale production without compromising its fundamental superparamagnetic nature is an essential element associated for clinically significant magnetic nanoparticles.

The aggregation of bare SPION is basically attributed to the Van der Waals forces and the magnetic dipolar interactions associated with materials showing ferromagnetic property.[23] Surface functionalization is very essential and is a generally used method to impart long term stability as well as biofunctionality to the nanoparticles.[24,25,26] Among the diverse surface modification techniques, use of an inorganic matrix is recognized as an effective method for imparting uniform particle size to the magnetic nanocrystals[27,28] by formulating a

homogeneous dispersion of the precursors. Recently the authors have developed superparamagnetic nanocomposite consisting of very uniform size of SPIONs homogenously embedded by hydroxyapatite nanoparticles.[29] Also the iron oxide incorporated HA has systematically evaluated the biofunctional properties such as cellular interaction, gene delivery, bone regeneration and hyperthermia therapy.[30,31,32] Hydroxyapatite (Ca_{10} $(PO_4)_6$ $(OH)_2$) has been well recognized as one of the most biocompatible bioceramic material used for several clinical applications.[33,34] The various weight percentage magnetic and non-magnetic phases of compositions of nanocomposite were synthesized through co-precipitation route. The various physicochemical characterizations were investigated for understanding the phase purity, nature of bonding, magnetic property and percentage of compositions of nanocomposite. The present study highlights the unique behaviour of the above nano magnetic bioceramic particles towards some specific cells. For biocompatibility evaluation, the minimum iron oxide embedded with better magnetic property of HAIO50 (50wt% of nonmagnetic phase of HA) was subjected to *in vitro* cell-material interaction studies. The various concentrations of HAIO50 were used for cell separation from the biological suspension. HeLa cells were selected as a model cell separation experiment. Role of concentration as well as time in enabling cell labelling was quantitatively evaluated using HAIO50 nanoparticles. The HAIO50 labelled cells were effectively separated and cultured. The design is depicted schematically in the Fig. 1. Our results demonstrate an efficient non-invasive mode of cell therapy with SPION embedded HA with the aid of external magnetic field.

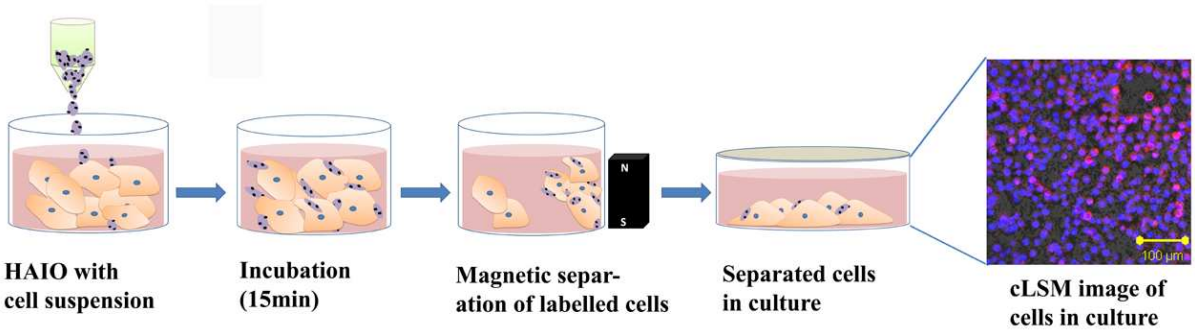

Fig. 1 Schematic illustration of the magnetic nanocomposite HAIO50 based cell suspension labelling, separation and culturing under *in vitro* condition.

2. Materials and method

Samples of $FeCl_2 \cdot 4H_2O$ (Merck, Darmstadt, Germany), $FeCl_3$ (Merck), $Ca(NO_3)_2 \cdot 4H_2O$ (Rankem, New Delhi, India), $(NH_4)\ H_2PO_4$ (Rankem), and 25% aqueous NH_4OH (SD Fine Chemicals, Mumbai, India) and 35% HCl (SD Fine Chemicals) were used as obtained 3-(4,5-Dimethyl thiazol-2-yl)-2,5 diphenyltetrazolium bromide (Sigma- Aldrich, USA), and streptomycin (Invitrogen, USA) Fetal bovine serum (Invitrogen, USA) were used for the MTT assay. All chemicals used for experiments other than mentioned in the material section were from the Sigma- Aldrich, USA.

2.1 Synthesis of iron oxide embedded hydroxyapatite (HAIO) composite and iron oxide (IO)

The synthesis of HAIOs was carried out by *in situ* co-precipitation of iron salts and calcium phosphate precursors in alkaline medium at elevated temperature. Briefly, the iron salts solution was freshly prepared in an acidic medium of HCl using $FeCl_2 \cdot 4H_2O$ and $FeCl_3$ in the ratio of 1:2. The $Ca\ (NO_3)_2 \cdot\ 4H_2O$ and $(NH_4)\ H_2PO_4$ solutions were taken in such a way as to get the Ca/P ratio of 1.67. The $Ca(NO_3)_2 \cdot 4H_2O$ solution was mixed with iron salt solution with constant stirring. The pH of the above solution was then slowly increased up to 11 by

adding 25% ammonia solution together with $(NH_4)H_2PO_4$ for a period of 1h. The addition and mixing of reagents were done under N_2 atmosphere. The suspension was aged for 24h at room temperature, after which the precipitate was washed several times with distilled water and centrifuged to get neutral pH condition. The iron oxide to hydroxyapatite weight percentage ratios of 10-90 were synthesis by same method. Ascending order of weight percentage of iron oxide in composite represented as HAIO10, HAIO30, HAIO50, HAIO70, and HAIO90. Bare IO was also prepared by 1:2 ratios of ferrous, ferric chlorides in the same reaction condition for size, phase purity, and chemical structure comparison.

2.2 Physicochemical characterization of HAIOs and IO nano particles composite

High-resolution TEM (HRTEM) analysis was performed for evaluating morphology, crystal size and composition analysis. The TEM images and energy dispersive X-ray spectra (EDS) were collected on a JEOL JEM-2010F microscope operated at 300 kV. TEM samples were prepared by dropping highly dispersed HAIO magnetic nanocomposite sample (very low concentration) on to a copper grid successively dried at room temperature for 24h. The micro-scale morphology and the composition analysis of HAIO nanocomposite was investigated with the aid of ESEM (ESEM; Quanta 200, The Netherlands). Samples were prepared by dispersing in distilled water by ultrasonication for 2 minutes. A single drop of the above suspension was put on an aluminium stub and dried at room temperature followed by gold coating. The composition of magnetic nano composite was evaluated using energy dispersive X-ray spectroscopy. The phase purity of crystals of HA, IO and HAIOs nano composites was analyzed using X-ray diffractometer (Bruker, D8 advance, Karlsruhe, Germany) using the Cu$K\alpha$1 radiation operating at 40 kV and 30 mA current strength. The crystal structure was determined by analyzing the position and intensities of diffraction peak typically observed in the range of diffraction angle $2\theta = 20°–70°$ and at a scan rate of $4°min^{-1}$ with a step wise of 0.1°. The hydrodynamic size and surface charge of the nanocomposite

particles were analyzed using Dynamic Light Scattering (DLS) Particle Size Analyzer (Malvern Instruments Ltd, Worcestershire, UK) by dispersing the sample in distilled water using ultra sonic probe sonication. The Fourier transform infrared (FTIR) spectra of the samples were collected on Thermo-Nicolet 5700 spectrometer. As the ceramic powder was found opaque to IR, diffuse reflectance (DRIFT) technique was used for measurement. Samples were dried and the powder thus obtained was thoroughly mixed with IR grade KBr powder and recorded reflectance spectrum, wavelength in the range 400 to 4000 cm^{-1} at a resolution of 4 cm^{-1}. KBr powder alone was used for background spectra. Freeze dried powder samples were used for the magnetic property analysis. Vibrating sample magnetometry (VSM) was used to measure the magnetic properties of IO and HAIOs using a PAR EG&G Model 4500 magnetometer with an external field varying from -15 to 15 kOe at room temperature. The magnetization of each samples obtained as a function of the applied field.

2.3 In vitro biocompatibility

HeLa (human cervical carcinoma) cells were cultured in Dulbecco's Modified Eagle's Medium – High Glucose (DMEM -HG) with 10% Fetal Bovine Serum (FBS), 50 units ml^{-1} of penicillin and 50 μg ml^{-1} of streptomycin. All reagents were sourced from Invitrogen, India and cell culture lab ware from NUNC, Denmark. Cells were seeded and maintained at 37°C and 5% CO_2 atmosphere and experiments performed at 80% confluence.

2.3.1 Cell viability MTT assay

Viability of HeLa cells was ascertained using standard methyl thiazol tetrazolium bromide (MTT) assay as per Mossman et al[35] using HeLa fibroblasts. The nanocomposites HAIO10, HAIO30, HAIO50, HAIO70, HAIO90, IO and control were added to wells at final concentrations: 0.75mg and 1.5mg. After 24 hours incubation with above concentrations of

nanoparticles, MTT was added to each well, resulting formazan dissolved and optical density evaluated at 570 nm in a Chameleon Microplate Reader. Control in MTT experiment was Hela cells without exposure to particles. Control MTT activity was taken as 100% and test values plotted against it.

2.3.2 *In-vitro* Haemocompatibility

Samples were diluted with PBS (pH 7.4) to 10mg/ml hemoglobin concentration and performed the test. Samples as listed (HAIO10, HAIO30 & HAIO50) were used for the test and each sample at different test concentrations (0.1mg, 0.3mg and 0.5mg) was incubated individually with 100µL of whole blood having hemoglobin concentration 10mg/mL for 3h at 37^{o}C in a shaking water bath. The samples after centrifugation at 700-800 g for 15 min, the supernatant was observed for any released hemoglobin at 540 nm using methemoglobin test. The test was validated against Triton X100 as positive control and polyethylene glycol as negative control. The percentage of hemolysis was calculated by relative method based on Optical Density (OD). The experiments were run in triplicate and were repeated twice.

$$\text{Percentage hemolysis} = \frac{\text{Supernatant Hb released} * 100 * 8(\text{dilution factor})}{\text{Total Hb conc. of dil. blood}}$$

The calculated percentages of hemolysis for all the samples were compared with ASTM standard[36] which defines as highly hemocompatible (<5% hemolysis), hemocompatible (within 10% hemolysis) and nonhemocompatible (>20% hemolysis).

2.3.3 Cellular uptake - Prussian Blue Staining and flow cytometry evaluations.

Cells after post-incubation with nanoparticles were visualized with Prussian Blue staining method to detect the presence of iron. HeLa cells were grown on round glass coverslips (Blue Star, India) and incubated with HAIO50 nanoparticles (120µg) for 4 hours. After incubation, the coverslips were washed with sterile phosphate buffered saline and fixed with 95%

ethanol. Prussian blue staining was carried out with equal volume of 2% hydrochloric acid and potassium ferricyanide trihydrate for 15 min followed by washing with distilled water and images were captured on a Leica DMIL microscope. Cell interaction with the nanomaterial was analyzed using flow cytometry. HAIO50 was used for analysis at varying concentrations (30µg, 60µg, 120µg, 240µg, 480µg and 960µg). $1x10^6$ HeLa cells in suspension were treated with the nanoparticles at 15mins and measured forward scatter (FSC) and side scatter (SSC) collected on a Becton Dickinson FACS Aria instrument using FACS ARIA software.

2.4 Cell Separation

HeLa cells ($1.4x10^3 cells\mu l^{-1}$) were added to seven tubes (A-G) and incubated for 15 minutes with varying concentrations of HAIO50 (C1 to C6) in PBS. Cells were pre-stained with Acridine Orange and magnetic separation carried out with external magnet (0.3T) for 1 minute to all tubes. Supernatant and pellet was collected into separate tubes. Cell number was evaluated using Coulter counting (Sysmex K-4500). Supernatant & pellet resuspended in 500 µl PBS and placed on an UV – Transilluminator (Bangalore, Genei).

2.4.1 Morphological Study – Cell Separation:

To understand effect of cell separation dynamics on cell morphology imaging studies were carried out. Pellet isolated via magnetic separation was fixed in 1% glutaraldehyde (Electron Microscopy Sciences) overnight. The pellet was prepared as a thin film on a clean glass slide (Blue Star, India) and dried at room temperature. The film was fixed in 100% methanol, air – dried and stained with Giemsa Stain (1:20 volume dilution). Excess stain removed by washing with diluted buffer solution, dried and imaged under an inverted phase contrast microscope (Leitz DMIL, Leica, Germany). Environmental Scanning Electron Microscopy

(FEI QUANTA 200) was carried out on fixed pellets dehydrated in an ascending alcohol series and placed on a glass coverslip.

2.5 Cell culture of magnetic separated cells

Cell pellets collected by magnetic separation were transferred into culture wells under aseptic conditions and provided with growth medium (DMEM – HG) and culture maintained for 24 hours. Cell morphology was collected using a Leica DMIL inverted microscope.

2.5.1 Cytoskeleton, morphology evaluations by Confocal laser scanning microscopy (CLSM) and Environmental Scanning Electron Microscopy (ESEM)

The F- actin structure and morphology of the magnetically separated cells, after 24h culture, were observed by confocal laser scanning microscopy and Environmental scanning electron microscopy. For CLSM evaluation, the monolayered cells were fixed in 4% paraformaldehyde and permeabilized with 0.25% Triton X-100 for F-actin staining in the cells. F-actin was stained with Alexa-fluor-488-phalloidin and the nucleus was counterstained with 4',6-diamidino-2-phenylindole (DAPI). The control and HAIO50-labeled HeLa cells were investigated using a confocal laser scanning microscope (Carl Zeiss LSM 510 META equipped with differential interference contrast optics). Images of the samples were prepared in multi-track mode with separate excitation of DAPI and Alexa-fluor-488-phalloidin.

3. Results and Discussion

The magnetic composite has been synthesized through common wet-precipitation technique that favours formation of nanoparticles. In principle, iron oxide (IO) nanoparticles are primarily formed and its charged surface subsequently initiates the nucleation of amorphous calcium phosphate nucleation. This initial calcium phosphate precursor layer is the key step that facilitates the embedding of iron oxide particle, which later on transforms to

apatite matrix. In addition, the initial adsorption of calcium phosphate prevents self-agglomeration of IO particles and hence uniformly distributed IO nanoparticles embedded by calcium phosphate matrix could be achieved. The same experimental conditions are applied for synthesizing different compositions of magnetic nanocomposites. It should be noted that the weight percentage ratio plays a critical role not only in determining the fundamental magnetic behaviour but also influence significantly on the crystal shape and growth pattern of the particles. Transmission electron as well as scanning electron microscopic evaluation imparts interesting information on the morphological features of various compositions of magnetic nanocomposite. Fig. 2 and Fig. 3 are the respective TEM and SEM micrographs, depicting the acicular or needle shaped crystals of hydroxyapatite containing IO nanoparticles within it.

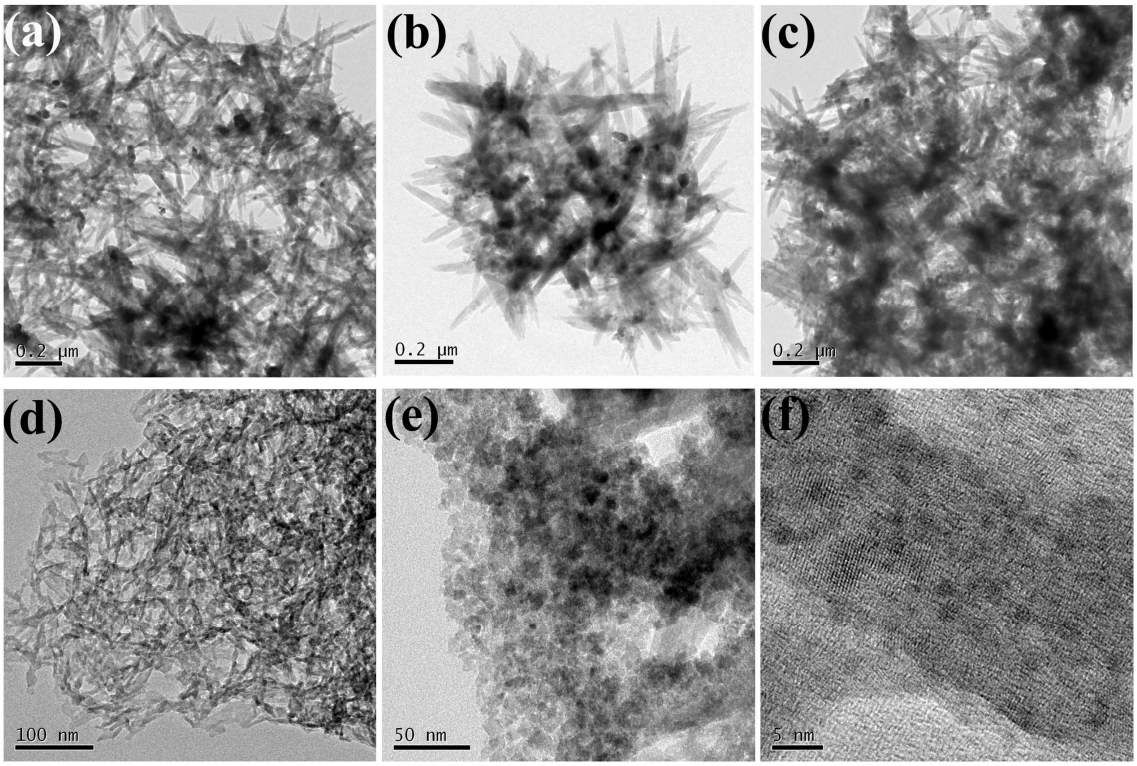

Fig. 2 Transmission Electron Micrographs of various weight percentage of IO embedded HA samples (a) HAIO10, (b) HAIO20, (c) HAIO30, (d) HAIO40, (e) HAIO50 and (f) higher magnification of (e).

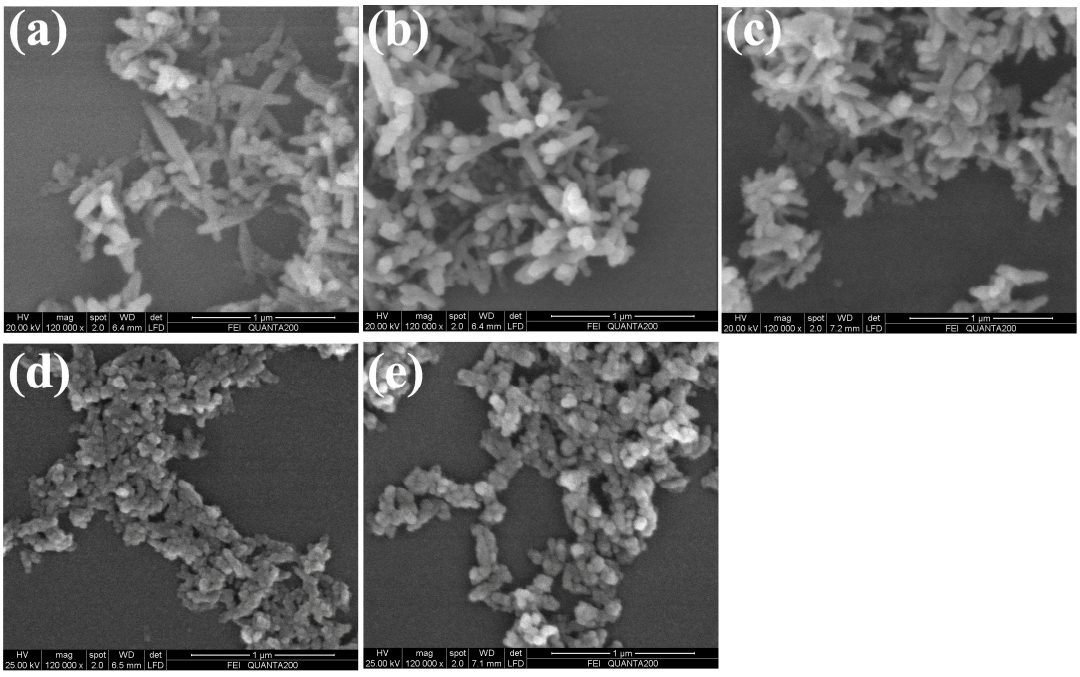

Fig. 3 Scanning Electron Micrographs of various weight percentages Iron Oxide (IO) embedded HA samples a) HAIO10 b) HAIO20 c) HAIO30 d) HAIO40 e) HAIO50.

It was observed that with increased concentration of IO particles, the shape and crystal growth pattern are altered, transforming from needle to spherical one. The lower concentrations of IO are 10, 20 and 30 wt% shows acicular nature of the crystals (as seen from Fig. 2a-c & Fig. 3a-c); while higher concentrations, 40 and 50wt % depicts the changes from acicular to spherical shaped HAIO composite (Fig. 2d,e & Fig. 3d,e). S-1Fig. 1a-e and S-2 Fig. 2a-e represent the EDS spectra of various compositions of HAIOs taken from the respective TEM and SEM micrographs. Corresponding peak intensities of iron, calcium and phosphorous elements in the EDS spectra shows good agreement to formation of all weight

percentage compositions. Moreover calcium and phosphorous peaks intensity ratio give the evidence of formation of hydroxyapatite nanocrystals irrespective of the presence of IO particles.

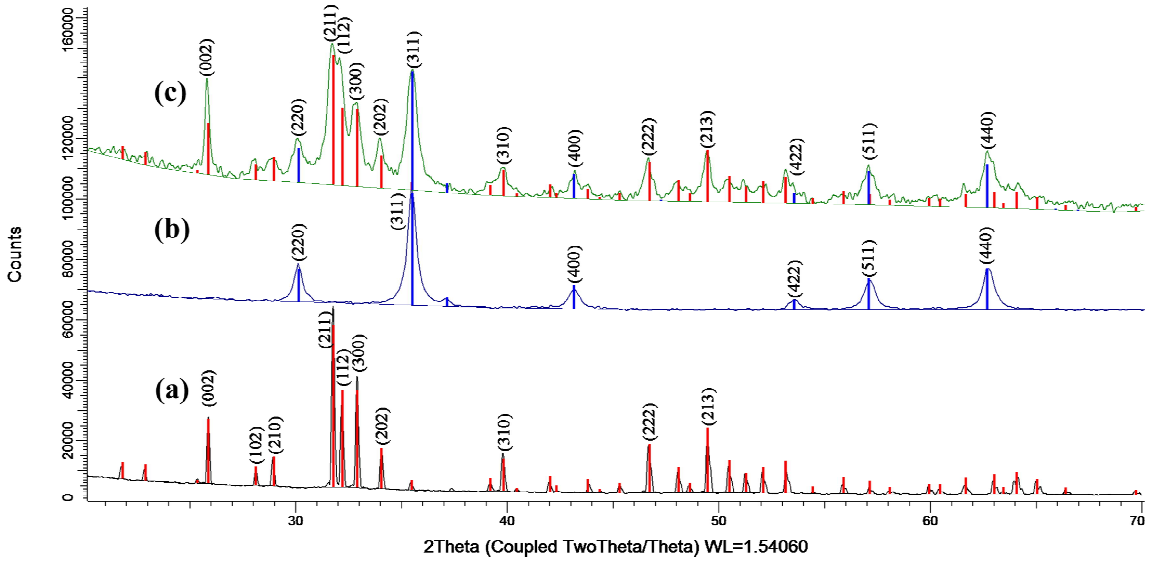

Fig. 4 X-ray Diffraction (XRD) pattern of a) HA b) IO c) HAIO50; [HA PDF= 00-009-0432, IO PDF= 01-071-6336].

The phase pure magnetic nanocomposite formation via this novel synthesis strategy was analysed by XRD as well as the FTIR spectroscopy. The XRD patterns of HAIO50 compared with HA and IO are demonstrated in Fig. 4a-c. The XRD pattern of HAIO50 revealed no secondary phases other than that normal hydroxyapatite and magnetite. The major peaks corresponding to HA (002), (211), (112), (300), (310), (222), and (213) and representative peaks of iron oxide (220), (311), (400), (422), (511), and (440) could be easily viewed from the spectra. The comparison with ICDD card number 01-071-6336 for iron oxide and 00-009-0432 for HA, data further confirms the presence of cubic spinal phase of nano iron oxide (Fe_3O_4) and hexagonal HA crystal structures. The various weight percentage composition of HAIOs XRD pattern depicted in S-3 Fig. 3a-d. When the percentage of iron

oxide increased, the peaks in the spectra broadened and decreased in intensity. This phenomenon was probably due to the small crystallite size and poor crystallinity of synthesized HAIOs.

The vibrational spectroscopic evaluation of samples was carried out with FTIR technique and represented in S-4 Fig. 4a-c. The FTIR spectra of HAIO50 composites with characteristic peak at 572cm^{-1} corresponding to stretching frequency of Fe-O bond of Fe_3O_4 crystals.[14] Moreover the vibration of hydroxyapatite such as the ν_1 (P–O) vibration of phosphate is observed as a peak at ~962 cm^{-1}. A peak at ~471 cm^{-1} is identified as the ν_2 (O–P–O) vibration of phosphate group. The peaks observed at ~1090 and ~1040 cm^{-1} have been identified as ν_3 (P–O anti-symmetric) vibrations. The ν_4 vibrations have been observed at ~604 and 567cm^{-1}. These characteristic peaks show the phase pure formation of magnetite embedded hydroxyapatite nano composite. Also from the analysis of various weight percentage compositions of HAIOs FTIR spectrum, it is indicated that there was no significant difference between the HA peaks and IO peaks, which demonstrate that the HAIOs kept its structure similar to phase pure HA and IO (S-5 Fig. 5a-d).

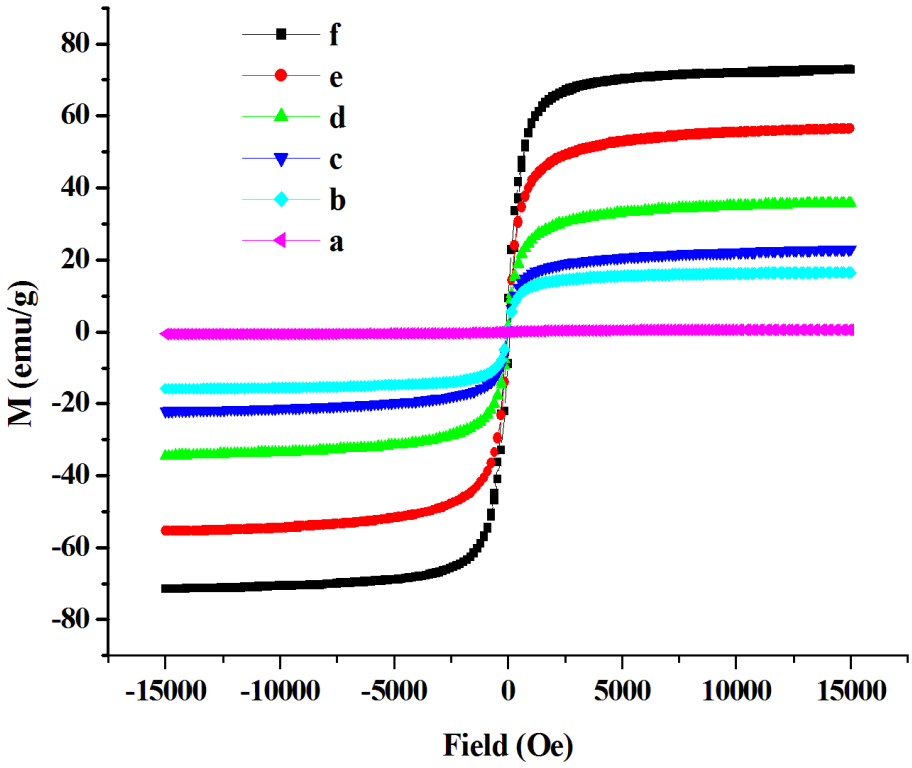

Fig. 5 Field-dependent magnetization curves (M-H) at 300K for magnetic composite with compositions of a)HAIO10 b)HAIO30 c) HAIO50 d)HAIO70 e)HAIO90 f)IO.

Magnetic measurements of HAIOs measured at room temperature are given in Fig. 5. The hysteresis displays no remanence and coercivity; which explain that the material compositions are possessing superparamagnetic nature with the absence of hysteresis curve. The superparamagnetic nature signifies that the magnetic particles embedded in the system are consisting of single domain nanocrystals and their magnetic moments are aligned in the direction of applied magnetic field. The bare iron oxide expresses highest magnetization value (73emu/g), and its corresponding composites decreases with lesser content of magnetic crystals in the composites nanoparticles. For application point, the HAIOs with lesser content of iron oxide with good magnetic response were observed in HAIO50. The HAIO50 shows magnetization value 23emu/g, which is suitable for cell separation application as it shows

optimal response and accumulates in the presence of external magnet. Moreover the stability of the HAIO50 was measured using zeta potential measurement and it is described in S-6 Fig. 6. The zeta potential value of the particle presents -14mV and it demonstrated the negative surface charge to HAIO50. The charged surface stabilizes the HAIO50 in the colloidal condition by electrostatic repulsion and it retains the dispersed state in prolonged time.[37,38,39]

Preliminary cytocompatibility of HAIOs was evaluated by MTT assay and hemocompatibility test. The MTT assay was used to measure cell viability after incubation with HAIO's. Cells were incubated with test samples for 24 hours and viability index was measured in percentage scale based on formazan production. S-7 Fig. 7 demonstrate that HAIO30, HAIO50, HAIO70 and HAIO90 nanoparticles are associated with very low toxicity when concentrations 0.75mg and 1.5mg were used over a period of 24 hours of exposure. The cytotoxicity effect of HAIOs compared with control values indicated not much variation with percentage of compositions and concentrations. It is noteworthy to mention that all the HAIOs concentration and compositions showed greater than 70% viability. Further, it is noteworthy to mention that, according to the higher concentration (1.5mg) of HAIOs used in the study has illustrated excellent viability and this concentration was very high dose than which further highlight the superior cell tolerance with these nanocomposite formulations.

A detailed biological evaluation was performed on lower weight percentage IO compositions of HAIOs, particularly due to increased interest associated with such compositions that holds lesser iron oxide content with optimal levels of magnetic activity. Haemolysis study was performed to assess blood compatibility of the candidate materials since intravenous route is the most commonly explored way of administration in practical scenario. Basic concern was interaction of the negative surface charge of HAIOs composites with cell membranes that has an inherent negative charge. Damage if any, resulting is expressed as percentage of haemoglobin release as shown in S-8 Table1.

The interactions of three different compositions of iron oxide hydroxyapatite [HAIO 10, HAIO 30 and HAIO 50] at three different concentrations (0.1mg, 0.3mg and 0.5mg) were exposed to hemolytic analysis. The result showed that all HAIOs with concentrations 0.1mg, 0.3mg and 0.5mg samples did not cause hemolysis as haemoglobin release levels were found to be well within the acceptable limits of hemocompatibility and cell viability for a biomaterial.[36] From these preliminary physicochemical and biological evaluations of HAIOs, the weight percentage ratio of 50:50 (HAIO50) with lesser content of IO showed better magnetic property, non toxicity and blood compatibility and hence it was selected for further biological evaluations.

Iron staining was carried out to evaluate the presence of magnetic nanoparticles 120µg of HAIO50 nanocomposite was incubated with HeLa cells followed by Prussian Blue staining. Iron staining is demonstrated as blue colour within cells. Presence of cytoplasmic inclusion of blue colour indicates uptake of particles in HeLa cells. As per S-9 Fig. 8, positive Prussian blue staining does not affect the morphology of the cells and they retain their native cellular structure *in vitro*, proving to be non-cytotoxic.

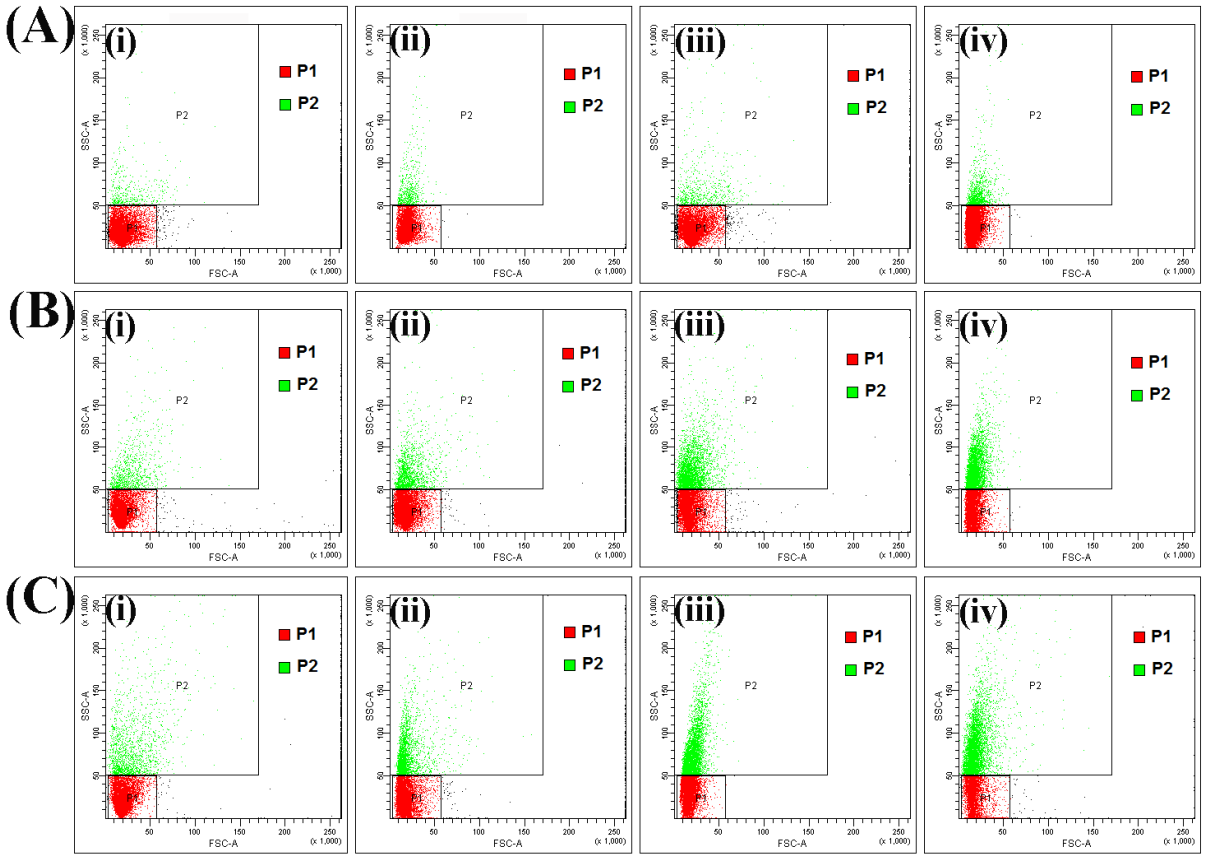

Fig. 6 FSC vs SSC plots of Flow Cytometric measurement of granularity change in HeLa cells; A, B & C are represents 120µg, 240 µg & 480 µg of HAIO50 in contact with 10^6 cells and (i), (ii), (iii) & (iv) indicated analysis at time points - 0,5, 10 & 15 min. P1= cells gated as Control indicated by no change in values P2= Cells in interaction with HAIO50 indicated by linearly correlated intensity of SSC channel. Plots indicate increase in uptake of HAIO50 from zero to fifteen min & a dose dependent response at longer time period with higher dosage.

Flow cytometric analysis was used to estimate cell – material interaction as a function of time with exposure to different doses of the nanoparticles. Side scatter is generally thought to be related to both the granularity of the cell and cell mass. The SSC signal is affected by the refractive index of the cytoplasm and number of organelles present in the cell.[40,41,42] Generally FSC provides the information of overall size of the cells. Approximately $1x10^6$

HeLa cells were treated with HAIO50 at 30, 60, 120, 240, 480 and 960 μg and held for time periods varying from T0 to T15 (minutes). Corresponding cellular interaction was assessed via changes in Forward Scatter (FSC) & Side Scatter (SSC). As indicated in Fig. 6 and S-11 Fig. 9 cell interaction, indicated by increase in SSC was based on HAIO50 concentration and incubation time. Control experiment was performed on a non–exposed population of cells, and cells gated as P1 (control) and P2. This helps differentiation of the cells in the absence of internalization of nanoparticles (P1) from those where there was a strong cell – material interaction. At lower concentrations 30, 60 and 120 μg the granularity changes [P2= 0.3, 0.6 and 1.2] were comparable to the control population even at 15 minutes of incubation. But at higher concentrations of HAIO50 240, 480 and 960 μg treated cells; the FSC was constant but the intensities of SSC was higher depending on incubation time as presented in S-10 Table 2 and S-12 Table 3. That is, cells which took up higher doses of nanoparticles showed higher intensities of SSC. FSC is routinely used as a measure of cellular size comparison, irregular cell shape or damage to the cell membrane. It could be presumed from the results that the surface charge enhanced uptake of HAIO50 without adversely affecting the cell-cytoskeleton confirmed from the FSC intensities. Hence it could be stated that HAIO50 favour uptake mechanisms by cells and hence could be explored for cell-separation applications based on its inherent magnetic properties.

Flow cytometric analyses results indicate that surface potential enhanced cell binding at 960μg levels signifying possible application in floating cell binding based magnetic separation. This sets apart from the majority wherein floating cell separation is achieved using magnetic nanoparticle based receptor - ligand conjugated interaction. To better explore HAIO50 as an efficient probe for floating cell separation from suspension and evaluate its potential as a carrier for cell therapy, low dose of HAIO50 nanoparticles (30, 60, 120, 240, 480, and 960μg) were incubated with Acridine Orange stained $1x10^6$ HeLa. Supernatant after

magnetic separation as well as pellet were subjected to analysis for cell population using a Coulter Cell Counter. A concentration of 480µg of HAIO50 was efficiently separated from all cell suspension with a 15 minute incubation period. To further understand the mechanism of interaction with nanoparticles, separation experiments were carried out 4^{o}C which would inhibit energy consuming processes similar to direct endocytosis of nanoparticles to the cells.[43] Separation efficiency of the 480µg dose preserved at 4^{o}C was found comparable to results performed at room temperature (Table 1) indicating an independent interaction mechanism.

Concentrations Of HAIO50 (µg)	**Supernatant cell count (HeLa *10^{3}cells)**	
	Temperature (25^{o}C)	**Temperature (4^{o}C)**
30	**1.4**	**2**
60	**0.8**	**1.6**
120	**0.6**	**1.4**
240	**0.3**	**0.6**
480	**0.2**	**0**
960	**0**	**0**

Table 1 The coulter counter cell count of supernatant from HAIO50 magnetically separated cells done at room temperature (25^{o}C) and low temperature (4^{o}C). Cells separated from suspension linearly decreased with concentration of material.

As cells are tagged with Acridine Orange, to ascertain the fluorescent intensity of supernatant and pellet; the magnetically separated stained Hela cells were placed under UV transilluminator. Images in S-13 Fig.10 dictated strong green fluorescence in the control tube while fluorescence was absent in supernatant from tubes B and C corresponding to 480µg and

960µg. Supernatant from tubes D through G; 240, 120, 60 and 30µg respectively showed increasing levels of fluorescence which further corroborate coulter counter observations of a residual cell population at lower particle concentration. To confirm cell separation into pellet compartment, pellets were re-suspended and observed under UV illumination. A dose dependent decrease in fluorescence for lowering dose could be visualized in S-13 Fig. 10.

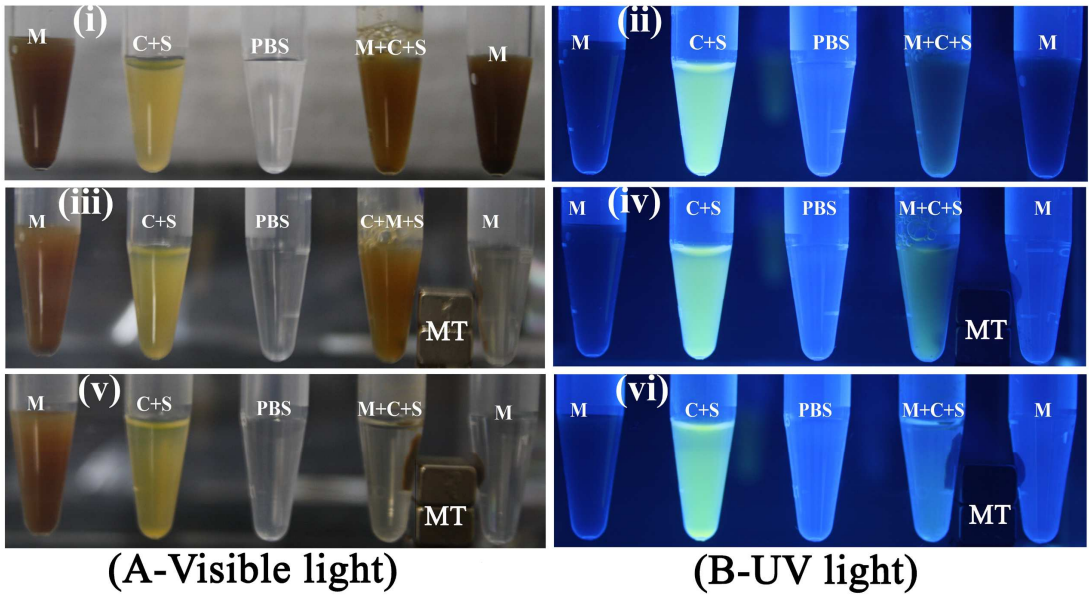

Fig. 7 Visible Light (A- i, iii, v) & UV (B - ii, iii, vi) Illumination of Acridine Orange (AO) stained HeLa cells incubated with HAIO50 for 15min and separated with an external magnet (MT) placed in the vicinity between 4th and 5th tubes [0.3T]: M=HAIO50 alone, C+S= cells stained with AO, PBS= buffer, M+C+S= stained cells and HAIO50. (i) & (ii) zero min (iii) & (iv) 2min, (v) & (vi) 10min, post magnetic exposure.

Cell separation techniques ideally should preserve cell morphology and integrity to help in the continued functionality of the cells after post- magnetic separation. In order to evaluate this, pellets containing cells after the optimal removal concentration of 240µg HAIO50 was evaluated by Giemsa staining and ESEM techniques.

Giemsa stained cells were viewed as dark purple colour under light microscopy as represented in S-14 Fig. 11, while the unattached cells on glass slide were observed as spherical units with a dark violet colour in both control and pellet. HAIO50 clumps appeared as dark yellow colour in both pellet and in bare sample. Characteristic spherical morphology of cells preserved in control and from cells recovered from pellet indicates a cell-friendly separation method. Environmental Scanning Electron Microscopy technique was further used to evaluate the smears of control and pellet recovered cells as depicted in Fig. 8. Separated cells were similar to corresponding control cell outlines, while those with adhered nanoparticle were visible on the cell surfaces and confirmed from corresponding EDS spectrum.

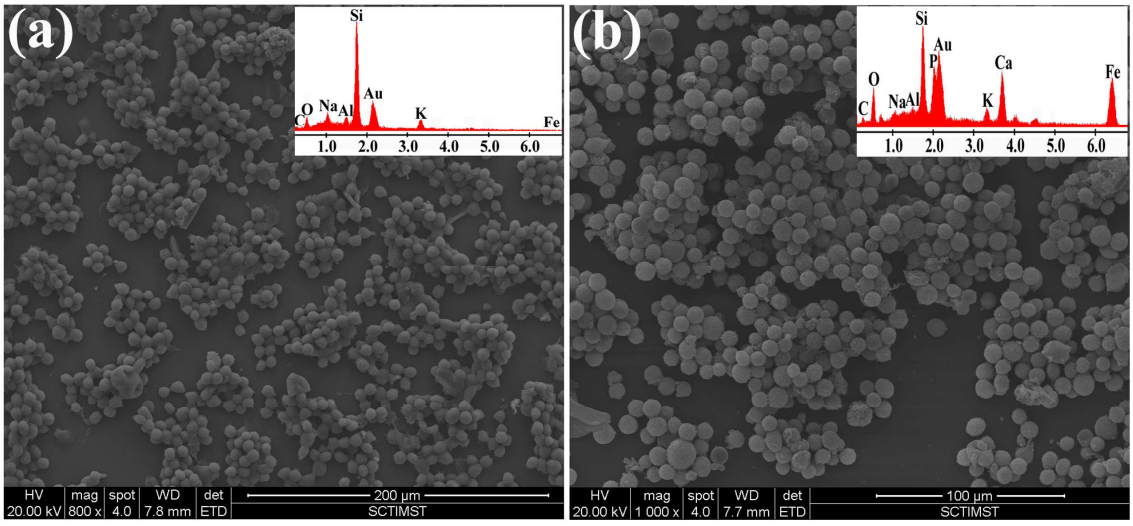

Fig. 8 Scanning Electron Micrographs: (a) Cells alone and (b) Magnetically Separated HAIO50 Cell pellet. The corresponding energy dispersive spectra are in inset.

Through magnetic accumulation induced cell therapy, an increase in the number of cells accumulation at injury site is reported.[44,45] But it is important to note that a continuous reduction in cell survival and localization at the target site occurs over time in previous studies.[11,46] In order to establish the efficacy of magnetic separated cells for cell therapy, and

to demonstrate a non - deleterious effect to cellular structure and functions, cells post – separation were maintained in culture. Cells separated using a 60µg HAIO50 dose and maintained under standard cell culture conditions for 24 hours post – separation. Actin staining and visualization using confocal laser scanning microscopy studies confirmed normal cytoplasmic skeletal organization (Fig. 9).

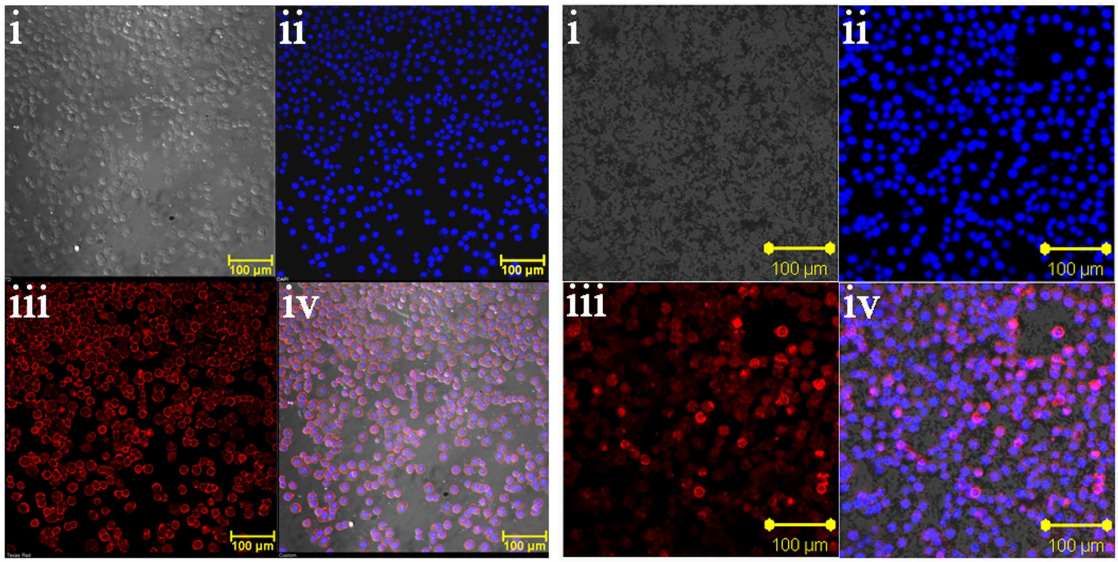

Fig. 9 Confocal Laser Scanning Micrographs of magnetically separated HAIO50 Cell pellet in culture for 24 hrs (i) in DIC mode (ii) DAPI (nuclei) stained cells (iii) Rhodamine Phalloidin stained Actin and (iv) merged image of (ii) & (iii). A – Control of cells alone and (B) Magnetically separated HAIO50 Cell pellet.

Individual actin fibres appeared as organized well-defined, clearly visible and HAIO50 particles are viewed as black intracellular spots. The depth and diameter of the cells were calculated from the 3-D reconstructed image of cells obtained from z-axis scans. From the actin cytoskeleton distribution evaluation, no structural change were observed for magnetically separated cells compared to control cells and fibrous structure with cell-cell

contact is observed only in biocompatible condition. Therefore the magnetic composite based cell separation and subsequent culture could be essentially employed as one of the efficient techniques for cell transplantation therapy.

4. Conclusion

In summary, we designed and fabricated novel type an intelligent magnetic nanopartcles for targeted site cell delivery. The biphasic magnetic nanocomposite consisting of magnetic Fe_3O_4 embedded in a matrix of Hydroxyapatite crystallites was synthesised by base induced aqueous chemical co-precipitation technique resulting in narrow size distributions. Synthesized HAIOs particles exhibit reliable superpramagnetic property Furthermore the nano composite consisted of 50% iron oxide, HAIO50, exhibited good magnetic hysteresis behaviour, biocompatibility and shown significant cell surface binding properties. Based on evaluations by coulter counter and UV- transilluminator, the capability to reliably separate the cells assembly from suspension is quantified and illustrated. More over the HAIO50 incorporated cells could be controlled by non-invasive magnetic field, concentrated separated and cultured under *in vitro* condition with no detectable impact on cell growth, proliferation & intracellular structures. Our results highlight the promise of using HAIO50 labelled cells as a new type of nanoprobe for remotely controlled cell therapies with better specificity and enhanced efficacy.

Acknowledgment

The authors express sincere thanks to the Director, SCTIMST and Head, BMT wing for the facilities provided. Also the authors thank Department of Science and Technology (DST), Govt. of India, for the financial support under ‘Synthesis of oxide based magnetic nanoparticles for biocompatibility studies, magnetic hyperthermia and MRI application

program. The support from Dr. Manoj Rama Varma, NIIST Trivardrum in the HR-TEM analysis and Dr. P. A. Joy, NCL,Pune in the VSM studies are also sincerely acknowledged.

References

1 H. W. Child, P. A. Del Pino, J. M. De La Fuente, A. S. Hursthouse, D. Stirling, M. Mullen, G. M. McPhee, C. Nixon, V. Jayawarna and C. C. Berry, *ACS Nano*, 2011, **5**, 7910–7919.

2 I. K. Herrmann, M. Urner, F. M. Koehler, M. Hasler, B. Roth-Z'Graggen, R. N. Grass, U. Ziegler, B. Beck-Schimmer and W. J. Stark, *Small*, 2010, **6**, 1388–1392.

3 H. B. Na, I. C. Song and T. Hyeon, *Adv. Mater.*, 2009, **21**, 2133–2148.

4 B. Mehdaoui, A. Meffre, J. Carrey, S. Lachaize, L.-M. Lacroix, M. Gougeon, B. Chaudret and M. Respaud, *Adv. Funct. Mater.*, 2011, **21**, 4573–4581.

5 Y. Li, J. Ma, H. Zhu, X. Gao, H. Dong and D. Shi, *ACS Appl. Mater. Interfaces*, 2013, **5**, 7227–7235.

6 D. K. Kim, M. Mikhaylova, F. H. Wang, J. Kehr, B. Bjelke, Y. Zhang, T. Tsakalakos and M. Muhammed, *Chem. Mater.*, 2003, **15**, 4343–4351.

7 Z. R. Stephen, F. M. Kievit and M. Zhang, *Mater Today (Kidlington)*, 2011, **14**, 330–338.

8 Y. Wang, *Theranostics*, 2013, **3**, 544–560.

9 O. Olsvik, T. Popovic, E. Skjerve, K. S. Cudjoe, E. Hornes, J. Ugelstad and M. Uhlen, *Clin Microbiol Rev*, 1994, **7**, 43–54.

10 D. J. Mooney and H. Vandenburgh, *Cell Stem Cell*, 2008, **2**, 205–213.

11 S.-H. Li, T. Y. Y. Lai, Z. Sun, M. Han, E. Moriyama, B. Wilson, S. Fazel, R. D. Weisel, T. Yau, J. C. Wu and R.-K. Li, *The Journal of Thoracic and Cardiovascular Surgery*, 2009, **137**, 1225–1233.e1.

12 J. P. Singh, *J Am Coll Cardiol Intv*, 2009, **2**, 803–804.

13 Z. Huang, N. Pei, Y. Wang, X. Xie, A. Sun, L. Shen, S. Zhang, X. Liu, Y. Zou, J. Qian and J. Ge, *Biomaterials*, 2010, **31**, 2130–2140.

14 J. Chen, N. Huang, B. Ma, M. F. Maitz, J. Wang, J. Li, Q. Li, Y. Zhao, K. Xiong and X. Liu, *ACS Appl. Mater. Interfaces*, 2013, **5**, 5976–5985.

15 M. Edmundson, N. T. Thanh and B. Song, *Theranostics*, 2013, **3**, 573–582.

16 S. Kubinová and E. Syková, *Nanomedicine (Lond)*, 2010, **5**, 99–108.

17 J. W. M. Bulte, S.-C. Zhang, P. van Gelderen, V. Herynek, E. K. Jordan, I. D. Duncan and J. A. Frank, *Proc Natl Acad Sci U S A*, 1999, **96**, 15256–15261.

18 K. Andreas, R. Georgieva, M. Ladwig, S. Mueller, M. Notter, M. Sittinger and J. Ringe, *Biomaterials*, 2012, **33**, 4515–4525.

19 P. G. Kyrtatos, P. Lehtolainen, M. Junemann-Ramirez, A. Garcia-Prieto, A. N. Price, J. F. Martin, D. G. Gadian, Q. A. Pankhurst and M. F. Lythgoe, *JACC Cardiovasc Interv*, 2009, **2**, 794–802.

20 R. Handgretinger, P. Lang, M. Schumm, G. Taylor, S. Neu, E. Koscielnak, D. Niethammer and T. Klingebiel, *Bone Marrow Transplant.*, 1998, **21**, 987–993.

21 U. Schoepf, E. M. Marecos, R. J. Melder, R. K. Jain and R. Weissleder, *BioTechniques*, 1998, **24**, 642–646, 648–651.

22 L. Kou, J. Sun, Y. Zhai and Z. He, *Asian Journal of Pharmaceutical Sciences*, 2013, **8**, 1–10.

23 S. Manju, C. P. Sharma and K. Sreenivasan, *J. Mater. Chem.*, 2011, **21**, 15708–15717.

24 S. Liang, Y. Wang, J. Yu, C. Zhang, J. Xia and D. Yin, *J Mater Sci Mater Med*, 2007, **18**, 2297–2302.

25 A. K. Gupta and M. Gupta, *Biomaterials*, 2005, **26**, 3995–4021.

26 A.-H. Lu, E. L. Salabas and F. Schüth, *Angew. Chem. Int. Ed. Engl.*, 2007, **46**, 1222–1244.

27 D. Dupont, W. Brullot, M. Bloemen, T. Verbiest and K. Binnemans, *ACS Appl Mater Interfaces*, 2014, **6**, 4980–4988.

28 E. M. Moreno, M. Zayat, M. P. Morales, C. J. Serna, A. Roig and D. Levy, *Langmuir*, 2002, **18**, 4972–4978.

29 E. B. Ansar, M. Ajeesh, Y. Yokogawa, W. Wunderlich and H. Varma, *J. Am. Ceram. Soc.*, 2012, **95**, 2695–2699.

30 H.-C. Wu, T.-W. Wang, M. C. Bohn, F.-H. Lin and M. Spector, *Adv. Funct. Mater.*, 2010, **20**, 67–77.

31 N. Tran and T. J. Webster, *Acta Biomater*, 2011, **7**, 1298–1306.

32 C.-H. Hou, S.-M. Hou, Y.-S. Hsueh, J. Lin, H.-C. Wu and F.-H. Lin, *Biomaterials*, 2009, **30**, 3956–3960.

33 H. V. Easwer, A. Rajeev, H. K. Varma, S. Vijayan and R. N. Bhattacharya, *Acta Neurochir (Wien)*, 2007, **149**, 481–485; discussion 485–486.

34 S. V. Dorozhkin and M. Epple, *Angewandte Chemie International Edition*, 2002, **41**, 3130–3146.

35 T. Mosmann, *Journal of Immunological Methods*, 1983, **65**, 55–63.

36 S. K. Roy Chowdhury, A. C. Kulkarni, A. Basak and S. K. Roy, *Wear*, 2007, **262**, 1387–1398.

37 M. R. Jahn, H. B. Andreasen, S. Fütterer, T. Nawroth, V. Schünemann, U. Kolb, W. Hofmeister, M. Muñoz, K. Bock, M. Meldal and P. Langguth, *European Journal of Pharmaceutics and Biopharmaceutics*, 2011, **78**, 480–491.

38 D.-H. Kim, Y. Guo, Z. Zhang, D. Procissi, J. Nicolai, R. A. Omary and A. C. Larson, *Adv. Healthcare Mater.*, 2013, n/a–n/a.

39 J. J. Thomas, M. R. Rekha and C. P. Sharma, *Colloids and Surfaces B: Biointerfaces*, 2010, **81**, 195–205.

40 A. Tzur, J. K. Moore, P. Jorgensen, H. M. Shapiro and M. W. Kirschner, *PLoS ONE*, 2011, **6**, e16053.

41 H. B. Steen, *Cytometry A*, 2004, **57**, 94–99.

42 R. M. Zucker, E. J. Massaro, K. M. Sanders, L. L. Degn and W. K. Boyes, *Cytometry A*, 2010, **77**, 677–685.

43 V. Sokolova, D. Kozlova, T. Knuschke, J. Buer, A. M. Westendorf and M. Epple, *Acta Biomater*, 2013, **9**, 7527–7535.

44 B. Polyak, I. Fishbein, M. Chorny, I. Alferiev, D. Williams, B. Yellen, G. Friedman and R. J. Levy, *Proc Natl Acad Sci U S A*, 2008, **105**, 698–703.

45 J. Riegler, J. A. Wells, P. G. Kyrtatos, A. N. Price, Q. A. Pankhurst and M. F. Lythgoe, *Biomaterials*, 2010, **31**, 5366–5371.

46 J. V. Terrovitis, R. R. Smith and E. Marbán, *Circ. Res.*, 2010, **106**, 479–494.